

A DEM BASED APPROACH TO UNDERSTAND THE PHYSICS IN SANDED WHEEL-RAIL CONTACTS

K. Six^{1,*}, W. Skipper², R. Lewis², B. Suhr¹

¹ Virtual Vehicle Research GmbH, Inffeldgasse 21a, 8010 Graz, Austria

² School of Mechanical, Aerospace and Civil Engineering, The University of Sheffield, Mappin Street, S1 3JD Sheffield, UK

* E-mail: klaus.six@v2c2.at

Abstract: A DEM model developed by the authors for sanded wheel-rail contacts, which considers the breakage of particles, the formation of sand clusters and the indentation of the surfaces, was used to investigate physical effects within the contact related to friction enhancement. The sand fragments were modelled in two ways: as spheres with blocked and with free rotation. For blocked spheres, relative motion between sand fragments and steel surfaces occurs, and the corresponding friction coefficient determines the overall adhesion coefficient. With this approach, High-Pressure Torsion (HPT) friction experiments could be reproduced. This was not possible for the case of rotating spheres; the adhesion could not be improved at all. Analyses showed that the ‘roller bearing’ effect is not responsible for this, but that shear forces occur in the opposite direction to the resulting overall shear force due to the rotation of the spheres. In addition, a mini shear box test rig was presented to further investigate the behaviour of sand fragments under high normal stresses.

Keywords: Wheel-rail contact, sanding, adhesion, low adhesion, traction, braking, DEM.

1. Introduction

In railways, the wheel-rail contact undergoes extremely high contact pressures and tangential stresses caused, for example, by traction or braking. The tangential force is limited by the maximal adhesion coefficient (AC) and under certain conditions, e.g., caused by water (‘wet-rail’ phenomenon) [1] or leaf layers in the contact [2][3], low adhesion occurs. Low adhesion interferes with traction and braking and is mitigated by wheel-rail sanding, where sand grains are blasted into the wheel-rail contact to raise the AC. The physical effects that cause this increase in the AC are still not fully understood.

Many experimental studies have been conducted on wheel-rail sanding; an overview can be found in references [4] and [5]. There are few numerical models in the literature that consider local effects in the wheel-rail contact region during sanding. These models focus on electrical isolation, which hinders train detection and can lead to safety problems [6][7], or particle entrainment efficiency [8][9][10].

Three very recent approaches aim to model the wheel-rail sanding process using particle-based approaches. In

reference [11], adhesion enhancement in a sanded wheel-rail contact is simulated using a two-dimensional Finite Element Method (FEM) model. The sand grains are modelled as triangles connected by so-called Cohesive Interface Elements, which allow for particle breakage. Although the model was able to reproduce some of the physical effects observed in the experiment qualitatively, the authors did not present a quantitative comparison of the adhesion with the experimental data.

In [12], a Discrete Element Method (DEM [13]) model of sanded High-Pressure Torsion (HPT) friction tests under dry conditions is presented. A sand grain is modelled using bonds between equally sized spheres that allow for particle breakage. The wheel and rail specimens are modelled as undeformable plates and regular grids of spheres, respectively. Contact between the wheel and rail specimens is ignored. Under dry conditions, experimental results show little difference in adhesion between sanded and unsanded cases. The simulation results are in good agreement with the measured adhesion. Furthermore, variations in bond parameters, such as, initial sand grain size, and the number of sand grains in the test are demonstrated. Bond parameters naturally influence breakage behaviour, and bond stiffness also strongly influences simulated adhesion. As the initial sand grain size increases, the simulated adhesion decreases; however, this effect could not be observed in the experimental results.

In [14][15][16][17], the authors of this study developed a DEM model of wheel-rail sanding. HPT tests under wet contact conditions were used to study wheel-rail sanding under laboratory conditions for two different types of rail sands called ‘GB’ and ‘AT’ under 900 MPa normal stress, see Figure 1 (c). Both types of sand show an increase in adhesion, interestingly the ‘GB’ sand performs better. To understand this behaviour, a DEM model of a HPT test was developed, which includes the experimentally observed processes: the repeated breakage of a sand grain, varying sand fragment spread, the formation of clusters of crushed sand powders, the plastic deformation of the steel plates due to the high load applied and the shearing of the sample under constant normal load, see Figure 1. The model developed is able to describe at least qualitatively the different adhesion improvement of the two sand types.

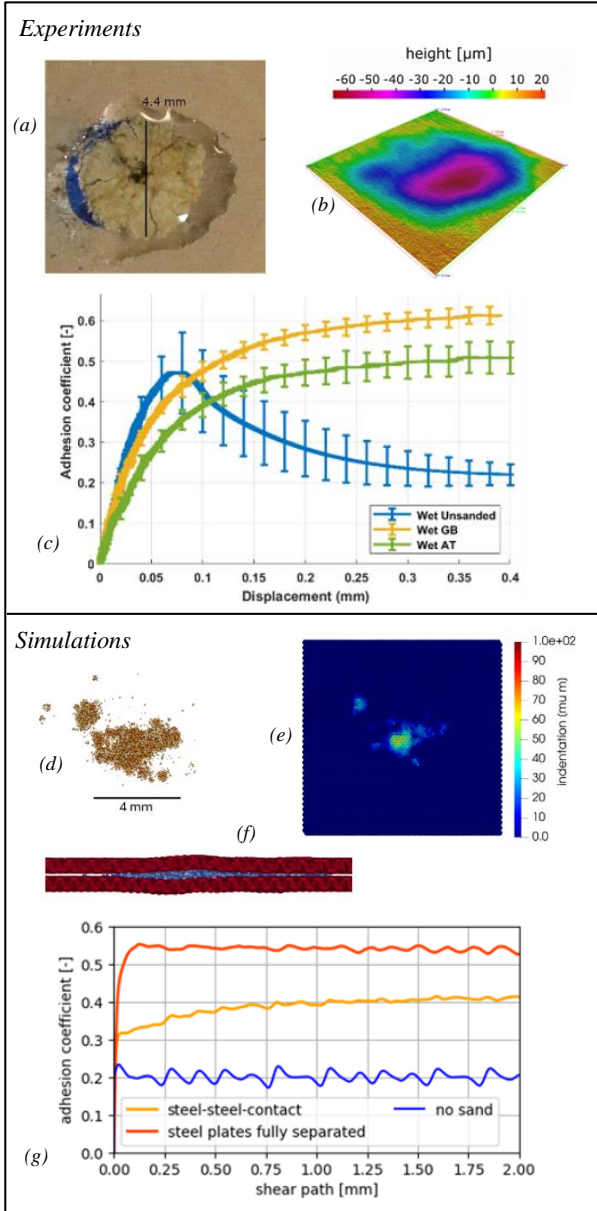


Figure 1 Experiments: (a) single grain crushing test with water, (b) indented steel surface, (c) HPT test measurements under wet conditions. DEM simulations: (d) crushed sand grain, (e) indented surface top view, (f) cut through sample during shearing, (g) simulated adhesion values. For details see [14][15][16][17].

A detailed description of the experimental and modelling work can be found in [14][15][16][17]. The focus in this work is on the physical effects which lead to the adhesion increase during the shearing of the crushed sand between the two indented surfaces.

2. Selected DEM results and discussion

The DEM model presented in [14][15][16][17] considers the repeated breakage of a sand grain, varying sand fragment spread, the formation of clusters of crushed sand powders and the plastic deformation of the steel plates due to the high loads applied. Sand grain breakage is modelled using the replacement method, wherein spheres representing the sand grains and their fragments are repeatedly replaced by smaller spheres once the strength limit is exceeded. Breakage stops below a certain radius, R_{lim} , to save calculation time. To conserve mass

after grain breakage, high sphere overlaps and thus high artificial energy are introduced. This energy is taken out of the system by an implemented freezing/unfreezing method of the particles, which contains a model parameter v_b that describes the maximum particle velocity at which the freezing of the particles is finished. To model the formation of sand fragment clusters, a phenomenological cohesive part in the particle-particle contact law is introduced, where the cohesion coefficient is much greater than that of normal cohesive materials. This part also influences the spreading behaviour. The cohesive part of the contact model includes two parameters, γ and R_γ . R_γ is the radius below which the crushed sand fragments behave cohesively; larger particles do not behave cohesively. High values of R_γ result in sticky fragment behaviour, leading to large clusters of sand fragments. Low values, on the other hand, correlate with strong spreading behaviour. Under wet contact conditions, the spread of fragments is reduced. This is considered in the model by adding a drag force, according to Stokes' law, to each particle. This introduces another model parameter: dynamic viscosity η , which was calibrated using experimental data. Surface indentation was modelled by describing the wheel and rail surfaces as overlapping spheres. When the stress on a surface sphere caused by the sand fragments exceeds its given hardness H , the surface sphere moves vertically. This method leads to an ideal plastic material behaviour. Unless otherwise mentioned, all simulations presented in this paper were performed with GB sand, small particles (diameter 1.18 mm) and the following parameters calibrated in [15]: $v_b = 0.12$ m/s, wet contact conditions ($\eta = 0.012$ Pas), $R_{lim} = 64$ μm , $\gamma = 800$ J/m² and $R_\gamma = 77$ μm . Furthermore, for all simulations the coefficient of friction for wet steel-steel contacts is set to 0.2 (baseline), see Figure 1 (c) 'Wet Unsanded' curve.

Figure 2 shows the results of HPT simulations, where the coefficient of friction in the sand-sand (μ_{SaSa}) and sand-steel contacts (μ_{SaSt}) is varied. The sand fragments are modelled as spheres with blocked rotation [15][16]. Two wheel-rail surface hardness's are considered, (a) hard $H = 10$ GPa and (b) soft $H = 2.5$ GPa. The bottom plots show how much of the applied normal load (90 kN corresponding to 900 MPa contact pressure) is carried by sand-steel contacts.

Two interesting results can be derived from these diagrams. For the case with hard surfaces the entire normal load is carried by sand-steel contacts while for the soft case about a third is carried by steel-steel contacts. The reason for this is that softer surfaces lead to deeper indentations and thus to more steel-steel contacts overall. The second interesting result is that increasing the coefficient of friction in sand-steel contacts has a greater positive effect on adhesion than an increase in the coefficient of friction for sand-sand contacts. Obviously, the relative movement between the sand powder and the steel surfaces at their interfaces dominates the frictional behaviour of sanded contacts. It was found that the combination of $\mu_{SaSa} = 0.5$ and $\mu_{SaSt} = 0.5$ yields simulation results closest to the experimental observations shown in Figure 1 (c) [17].

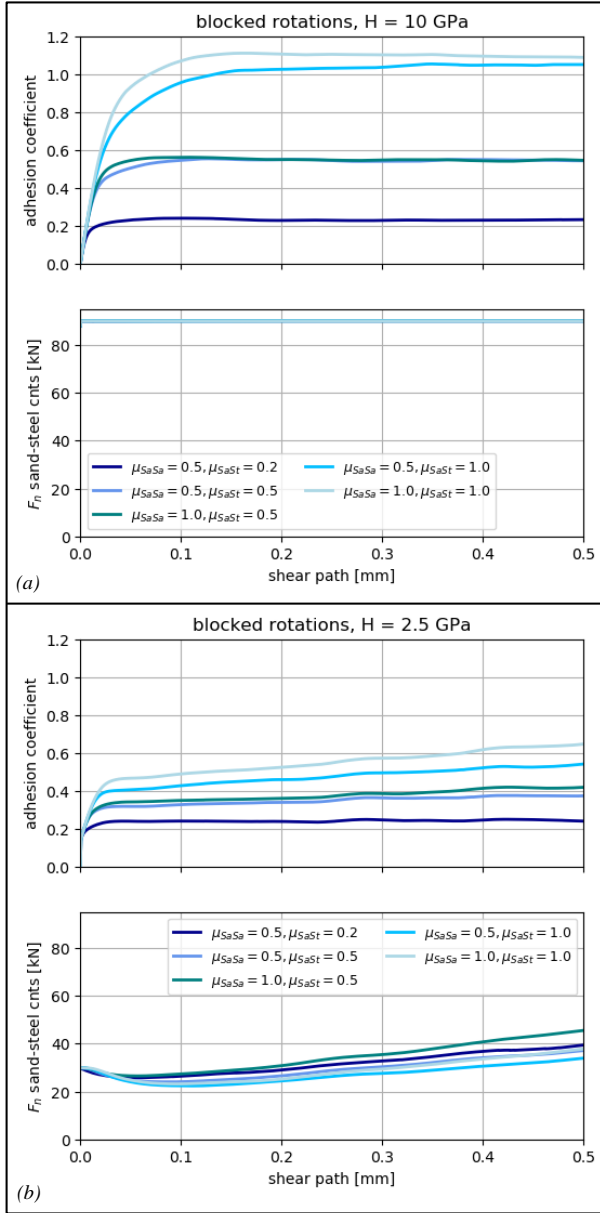


Figure 2 Adhesion coefficient and normal load transferred by sand-steel contacts simulated with varying friction in sand-sand and sand-steel contacts. Spheres with blocked rotation, (a) hard $H = 10$ GPa and (b) soft $H = 2.5$ GPa wheel-and rail surfaces [17].

To better understand the cause of this behaviour, the results of DEM simulations are analysed. Figure 3 shows two stages of the shearing process for sticky sand fragment behaviour ($R_f = 1$ m). Shearing starts when the full normal load is applied, this means the sand grain fractured repeatedly and indentations in the steel plates formed (at time t_0).

In Figure 3 (a) these indentations overlap fully/partially while in Figure 3 (b) this is no longer the case. Two individual particles are tracked during the shearing: particle 1 which is in contact with the bottom surface and particle 2 which is in contact with the top surface. At time t_1 , the upper surface has moved by Δs . At the same time both particles have moved from the left to right in shearing direction. Δs_1 and Δs_2 show the movement of the two particles relative to the surfaces they are in contact with. This relative movement generates frictional forces

dependent on the chosen coefficient of friction in sand-steel contacts. Remember, that the spheres representing sand fragments are not allowed to rotate. The qualitative sketch below shows the relative velocity situation and the qualitative velocity profile of the sand fragments between the two surfaces. Interestingly, no horizontal shear band in the plane of the undeformed surfaces develops through the compressed sand powder as the coefficient of friction in sand-sand contacts in combination with the interlocking effect of the particles prevents this. This is the reason why the coefficient of friction in sand-sand contacts has only a minor influence on the adhesion in the varied range (see Figure 2).

Figure 3 (b) shows the corresponding situation at a later point of the shearing process, where no overlap of the indentations exists anymore (from t_2 to t_3). Here the situation has completely changed. The particles in contact with the indented surfaces (3 and 6) do not move relative to the surface they are in contact with, while particles in contact with the unindented surfaces move relative to the surface with velocity v_t (velocity of the top surface). These results again emphasize the importance of the coefficient of friction in sand-steel contacts and the small influence of friction in sand-sand contacts.

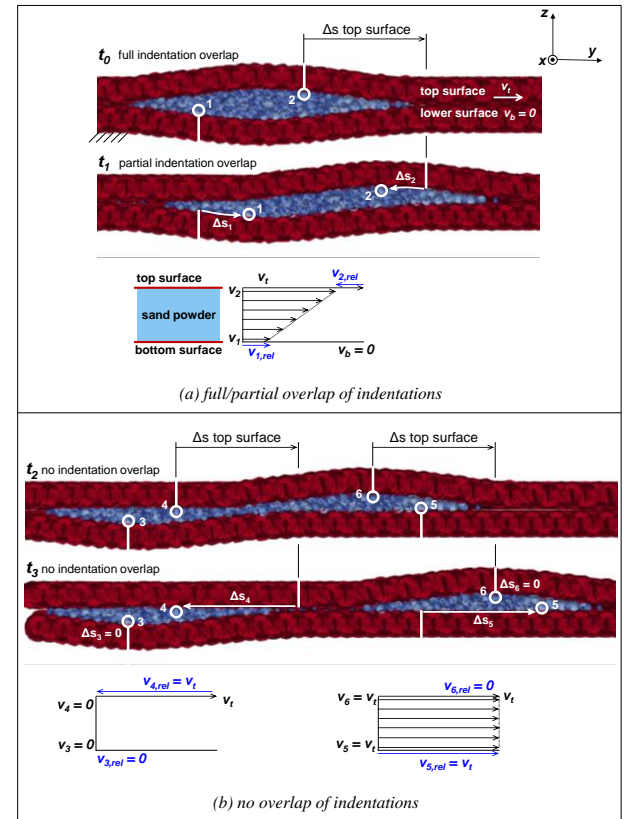


Figure 3 Relative movements between wheel and rail surfaces and sand-fragments at different phases of the shear motion: (a) full/partial and (b) no overlap of indentations. Top surface moves from the left to the right, bottom surface does not move. Spheres with blocked rotation, hard $H = 10$ GPa wheel-rail surfaces and sticky sand fragments ($R_f = 1$ m).

As mentioned above, the simulation results presented so far were produced using a model in which the sand fragments were considered as spheres with blocked rotation. However, in the real experiment, the fragments may rotate slightly during the shearing process, even if

they have a very angular shape, which may influence the resulting contact shear forces. This behaviour could be modelled as rotating spheres with rolling resistance. In this case, at least one additional model parameter would be introduced, which can lead to ambiguous parameter combinations if no proper experimental data is available. Aiming for simplicity of the model, this was avoided in [15][16]. However, to see what effects sand fragment rotation may introduce, the following extreme case was investigated: spheres representing sand fragments can freely rotate with no rolling resistance.

Figure 4 shows the results for this extreme case allowing free sphere rotation, comparable to results shown in Figure 2 for spheres with blocked rotation.

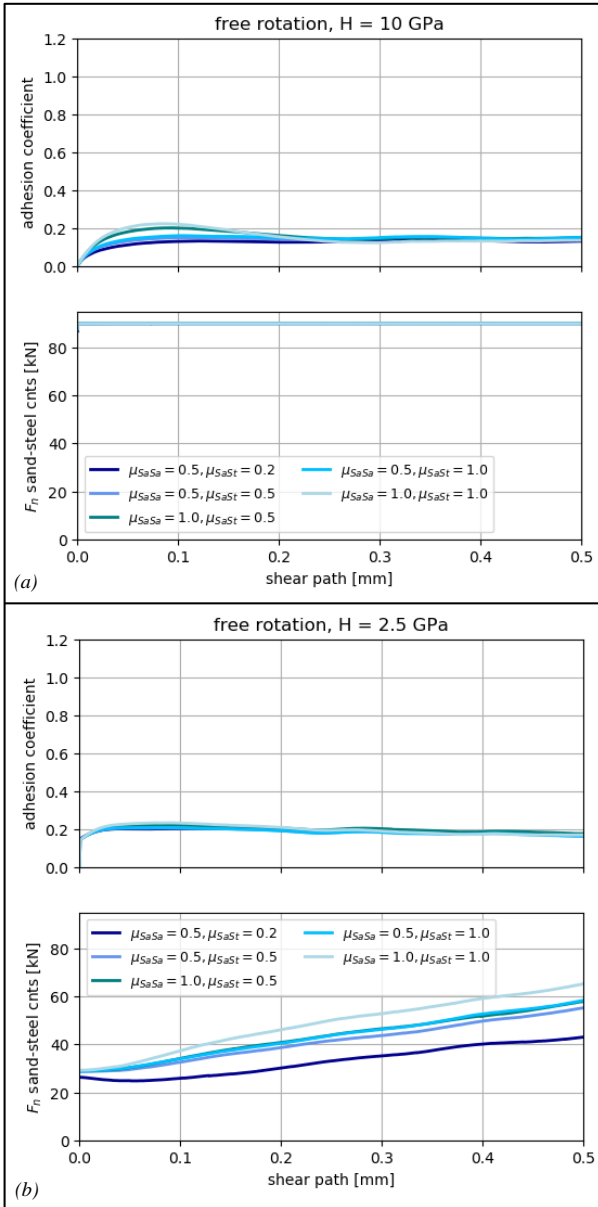


Figure 4 Adhesion coefficient and normal load transferred by sand-steel contacts simulated with varying friction in sand-sand and sand-steel contacts. Spheres with free rotation, (a) hard $H = 10$ GPa and (b) soft $H = 2.5$ GPa wheel-and rail surfaces.

In Figure 4, the portion of the normal load transferred via sand-steel contacts is the same – at least at the beginning

– as in the case with spheres with blocked rotations (compare with Figure 2).

For the hard surface case, no steel-steel contacts occur, and the applied normal load is fully carried by the sand-steel contacts. Interestingly, neither the coefficient of friction in the sand-sand contacts nor in the sand-steel contacts have a relevant influence on the adhesion coefficient. The harder surfaces show slightly lower values than the softer surfaces (compare (a) and (b)). This is in contrast to the results for spheres with blocked rotations, as shown in Figure 2. Even more, for the harder surfaces the calculated adhesion coefficient in some cases is even lower than the prescribed coefficient of friction for steel-steel contacts (0.2). One possible reason for this behaviour is that the spheres introduce a kind of roller bearing effect.

Figure 5 shows the median of the rotational angle of the sand particles around the x-axis (Φ) – see definition of coordinate system in Figure 3 – for the case of spheres with free rotation calculated as:

$$\phi = \int_0^t \omega_x dt \quad (1)$$

where ω_x is the angular velocity in x-direction. These results show that, as expected, rotation of the particles occurs. Comparing the results for hard surfaces (a) with the results for soft surfaces (b) reveals that in the case of hard surfaces the sand fragments tend to rotate more. This behaviour correlates with the slightly lower adhesion coefficients shown in Figure 4 (a).

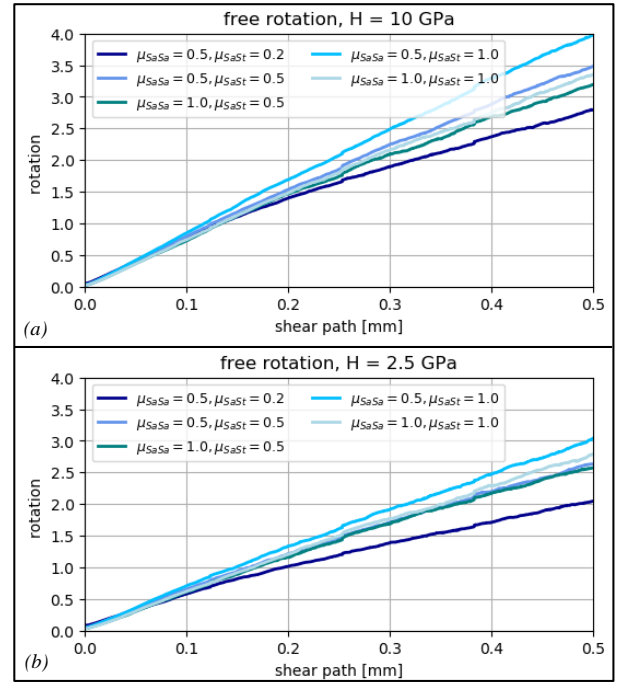


Figure 5 Median of the rotational angle of the sand particles with varying friction in sand-sand and sand-steel contacts. Spheres with free rotation, (a) hard $H = 10$ GPa and (b) soft $H = 2.5$ GPa wheel-and rail surfaces.

Figure 6 shows, for the case of rotating spheres, a cross section through the contact as in Figure 3 at a shear displacement of 0.35 mm for sticky sand fragments ($R_f = 1$ m). Analysing the history of the translational movement

of the particles in the y-z plane as in Figure 3 revealed that there is no difference compared to blocked spheres. However, due to it being possible for the particles to rotate, two regions with increased rotational angles develop, one near the top surface at the right, and one at the bottom surface at the left. Both regions show clockwise particle rotations (blue) which may contribute to the supposed “roller bearing” effect.

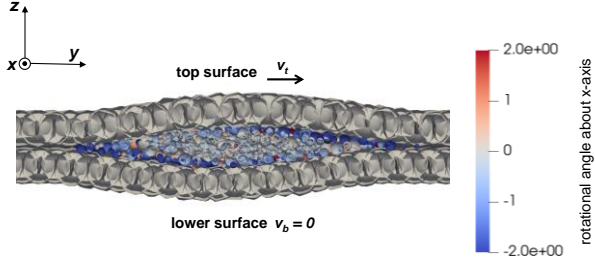


Figure 6 Cross section through contact as in Figure 3 at a shear displacement of 0.35 mm. Sand fragment colour shows rotational angle of particle around x-axis as defined in equation (1). Spheres with free rotation, hard $H = 10$ GPa wheel-rail surfaces and sticky sand fragments ($R_f = 1$ m).

Due to the rotation of the particles, one could assume that in this case more sliding in the sand-sand contacts occurs. Therefore, the so-called coefficients of mobilized friction (m_F) for sand-sand and sand-steel contacts were analysed. It is calculated for each contact as the absolute value of the tangential force (F_t) divided by the normal force (F_n) and then averaged for each contact group respectively:

$$m_F = \frac{1}{N} \sum_{i=1}^N \left| \frac{F_t^i}{F_n^i} \right| \quad (2)$$

Thus, mobilized friction ranges between 0 (no tangential force transferred) and μ (meaning all contacts are sliding). Figure 7 shows a comparison of the mobilized friction in sand-sand and sand-steel contacts for the hard surface case for spheres with (a) blocked and (b) free rotation. Mobilized friction of sand-sand contacts is very similar for cases of blocked and free rotation and is always below the prescribed coefficient of friction (0.5 and 1.0) meaning that not all contacts are in full sliding. This is a surprising result because a difference was expected due to the rotation of the sand spheres. In contrast, the values of mobilized friction in the sand-steel contacts clearly differ, the values for the case of spheres with blocked rotations are much higher than for the case with free rotation. For the case with blocked rotations the mobilized friction of the sand-steel contacts is close to the prescribed coefficients of friction in sand-steel contacts (0.2, 0.5, 1.0). This is different for the case with rotating spheres for $\mu_{SaSt} = 0.5$ and 1.0. However, the mobilized friction coefficients in the sand-steel contacts are still much higher than the corresponding adhesion coefficients, which needs further investigation.

Figure 8 shows the analogue results for the case of soft surfaces as in Figure 7. The same behaviour can be observed. Interestingly, there are also only minor quantitative differences in the mobilized friction, even if about one third of the normal load is transferred directly

via steel-steel contacts in the case of soft surfaces, as shown in Figure 2 (b).

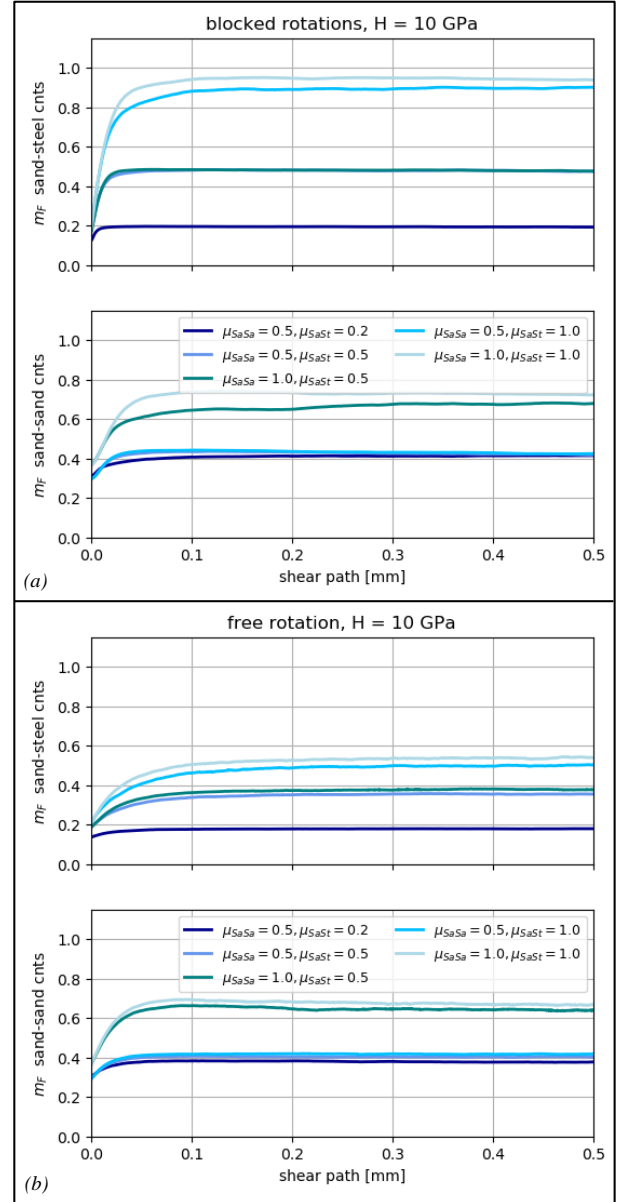


Figure 7 Mobilized friction in sand-sand and sand-steel contacts simulated with varying friction in sand-sand and sand-steel contacts. Hard surfaces $H = 10$ GPa, spheres with (a) blocked and (b) free rotation.

In a next step, the sand fragments that are in contact with the steel surfaces were divided into two groups for the case of spheres with free rotation: sand spheres which are in contact either with the top or the bottom surface only (spheres belonging to a multi-layer sand fragment cluster), and spheres which are in contact with the top and the bottom surfaces at the same time (spheres belonging to a single layer of sand fragments between the surfaces). The latter are assumed to contribute mainly to the aforementioned roller bearing effect. As shown in Figure 9 there is in both cases, hard and soft surfaces, a considerable portion of the normal load which is transferred by these ‘single-layer’ spheres. This portion is much higher for the case with hard surfaces, for which lower adhesion coefficients were also calculated. This indicates that the aforementioned roller bearing effect

could be responsible for the fact that no increase in adhesion can be achieved with rotating spheres. However, looking at the mobilized friction of the different groups of sand-steel contacts, the spheres that are in contact with both steel surfaces at the same time show lower values, but these values are still far from 0, which would correspond to the roller bearing effect. This in turn means that the roller bearing effect cannot be responsible for the ineffectiveness of the rotating spheres in terms of adhesion, but that there must be another physical reason for this.

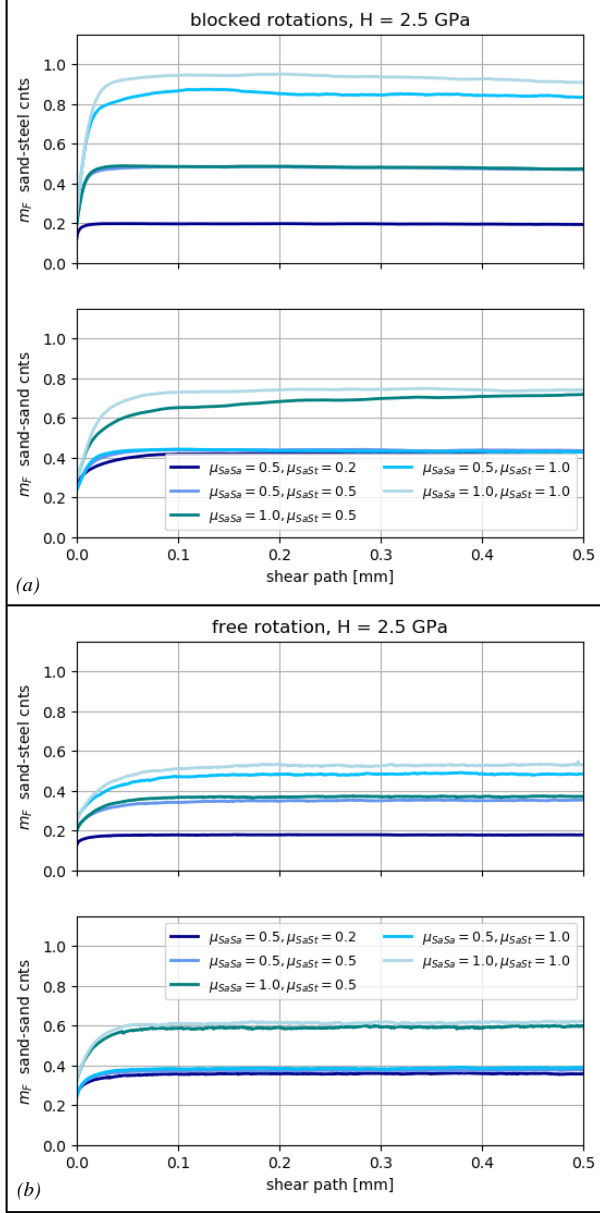


Figure 8 Mobilized friction in sand-sand and sand-steel contacts simulated with varying friction in sand-sand and sand-steel contacts. Hard surfaces $H = 2.5$ GPa, spheres with (a) blocked and (b) free rotation.

Next, the distribution of the tangential forces in sand-steel contacts on the top surface in shear direction (y) and perpendicular to it (x) are analysed. These force distributions were calculated at a shear path of 0.25 mm with $\mu_{SaSa} = \mu_{SaSt} = 0.5$. The results are shown in Figure 10. The first observation is that, as expected, all force

distributions in the shear plane perpendicular to the shear direction (x direction) are symmetrical about 0. This is of course not the case in shear direction (y direction) because overall shear forces are transmitted leading to the coefficient of adhesion.

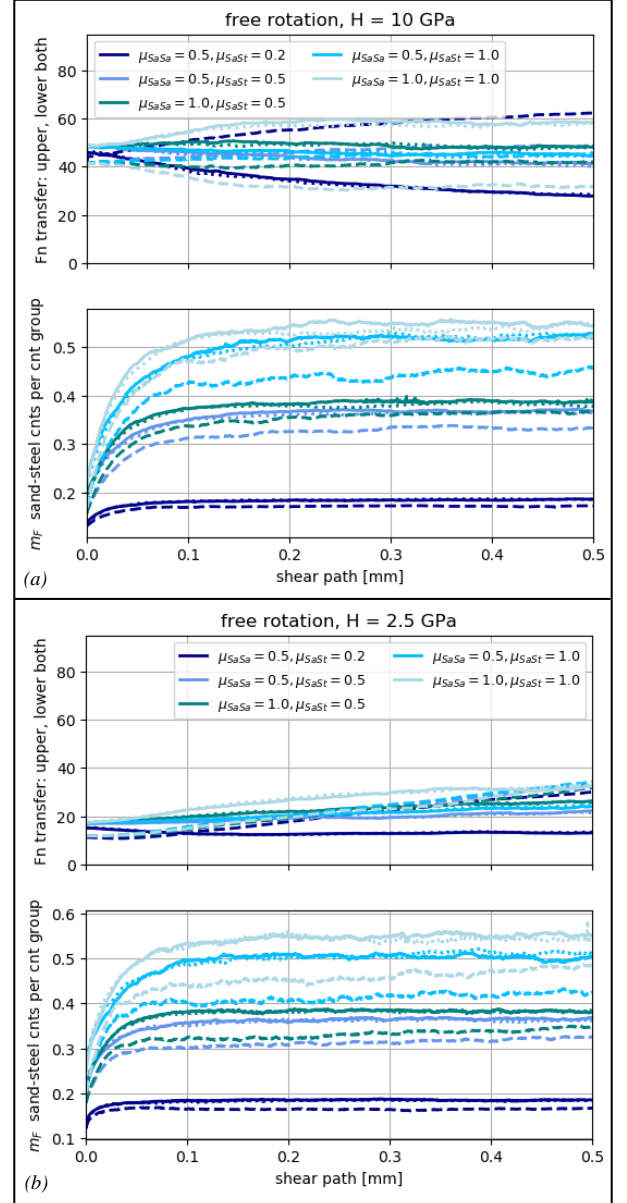


Figure 9 Portion of normal load and corresponding mobilized friction in sand-steel contacts where the sand spheres contact only the top surface (solid), only the bottom surface (dotted) or both (dashed). Simulations with varying friction in sand-sand and sand-steel contacts. Spheres with free rotation, (a) hard $H = 10$ GPa and (b) soft $H = 2.5$ GPa wheel-and rail surfaces.

However, there is one general difference comparing the cases with free rotating and blocked spheres. Blocked spheres show almost no negative forces which is very different for the free rotating spheres where a lot of negative shear forces occur. This behaviour explains the high mobilized friction coefficients for this case as shown in Figure 7 and Figure 8. There are still relevant shear forces in the sand-steel contacts, but many of them act in the opposite direction to the resulting shear force, thereby reducing the overall coefficient of adhesion. In addition,

the shear forces acting in the x-direction also contribute to the mobilized friction shown in Figure 7 and Figure 8.

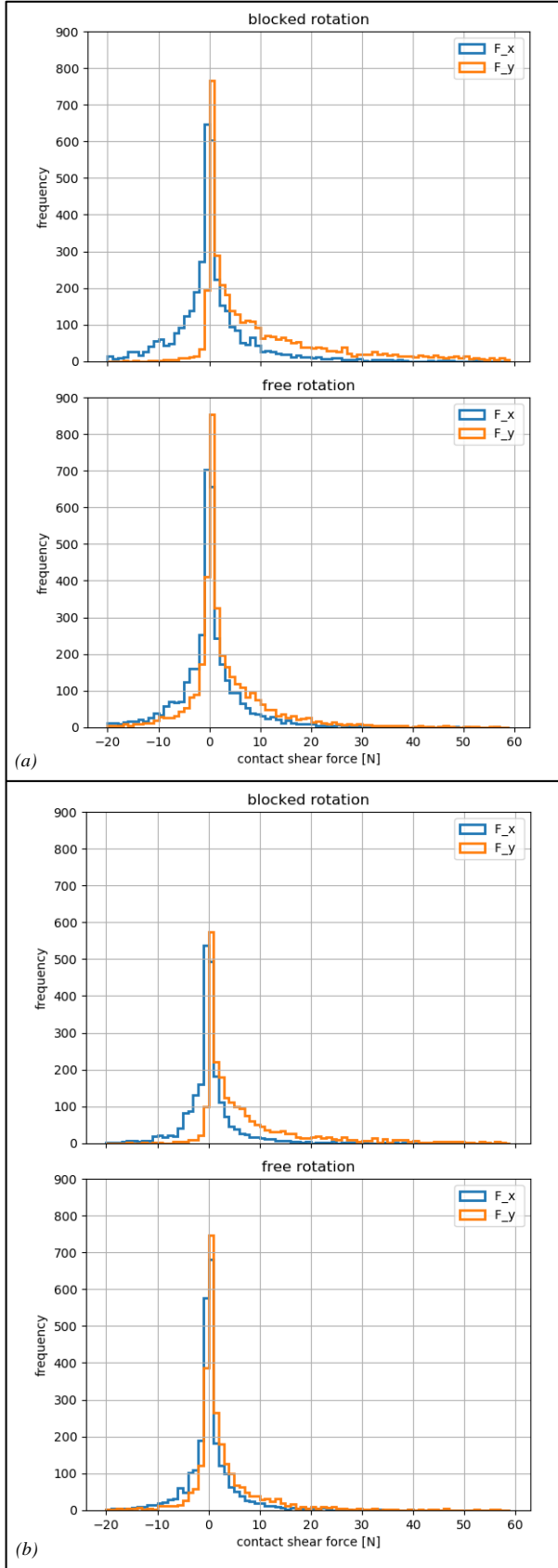


Figure 10 Distribution of tangential forces in sand-steel contacts on the top surface in shear direction (y) and perpendicular to it (x). Calculated at a shear path of 0.25 mm for the case of $\mu_{\text{SaSa}} = \mu_{\text{SaSt}} = 0.5$, (a) hard $H = 10$ GPa and (b) soft $H = 2.5$ GPa wheel-and rail surfaces.

There is no qualitative difference between the hard and the soft surface, only the frequency of the respective forces is lower in the case of the soft surface, as a part of the normal load is transmitted through steel-steel contacts.

In order to decide how the behaviour of sand fragments should be correctly modelled – blocked rotation, free rotation or rotation with rolling resistance – additional tests are required. For this reason, a new mini shear box test rig was developed, which is presented in the next section.

3. Mini shear box experiments

Figure 11 shows an image of the developed test rig and the schematic of how it works. First, sand grains are filled in. In the next step the vertical load corresponding to 300, 600 and 900 MPa which equates to 5.89, 11.78 and 17.67 kN (5 mm diameter) is applied. When the full vertical load is reached the height of the tablet like sand fragment specimen is about 4 mm. The test rig in vertical direction operates in force control. Vertical force and vertical displacement are measured and recorded. Here it is important to mention, that the measured vertical force, which is used by the controller, showed a dependency from the shear forces. This undesired behaviour is thought to be caused by the placement of the strain gauges used. Thus, the results presented here should be seen as indication, an error of up to 20% in the vertical force is possible.

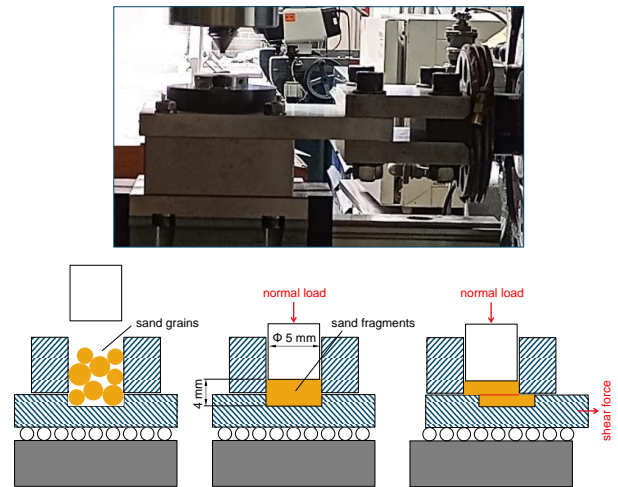


Figure 11 Image of the mini-shear box test rig (top) and scheme of how the test rig works (bottom).

Finally, the shearing of the specimen starts while the vertical load is kept constant. This is done in position control. Lateral displacement and lateral shear force are measured and recorded.

Figure 12 shows for GB sand the measured shear forces divided by the applied vertical forces (CoF) as a function of shear displacement. All three load cases show an initial increase up to a saturation point which is in the range between 0.4 and 0.55. After this point all curves show a decreasing characteristic which could be a result of the decreasing overlap of the upper and lower half of the sand-fragment specimen and therewith the increasing

effect from sand-steel contacts (see bottom right image in Figure 11). The initial gradient is the highest for the lowest load and lowest for the highest load. The test repetitions carried out for the three load cases show some scattering, however, the general behaviour is reproducible. The generated measurement data are freely available at zenodo.org, see [18].

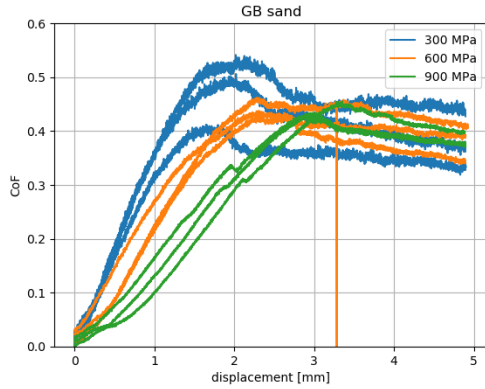


Figure 12 Coefficient of friction of crushed sand powder measured on a mini shear box test rig for three different vertical loads, each load case includes three repetitions.

Figure 13 shows two photos of the lower half of the compacted sand fragment sample after testing. Although the sand was crushed, some larger fragments are still visible. The reason for that could be a shielding effect – larger fragments are encapsulated by smaller ones – because several sand grains had to be filled in to achieve the desired height of the sand fragment sample. This will not occur in a real wheel-rail contact, where individual grains of sand normally pass through the contact and are crushed. In future tests, pre-crushed sand will be used, which should avoid this problem.



Figure 13 Crushed sand fragments and scratch marks on the lower lateral moving plane.

In a next step, it is planned to carry out DEM simulations for these experiments and compare them with the test data. This will make it possible to obtain an improved parameterisation for the modelling of the sand fragments described above. In addition, the aforementioned problem with the measurement of the vertical load must be solved in order to obtain more reliable test data.

4. Conclusions and future outlook

In this research physical phenomena occurring in sanded wheel-rail contacts were investigated with a DEM model which accounts for sand grain breakage, formation of

sand fragment clusters and the development of wheel-rail surface indentations. Two extreme cases of modelling the spheres representing sand fragments were considered, spheres with blocked rotation and spheres with free rotation. The first case represents the base line. This modelling approach was used in [15][16][17] and the calibrated DEM model was able to reproduce the coefficient of adhesion from HPT experiments and the difference between the two sand types (GB and AT). The main conclusions from this research are as follows:

- for blocked spheres no shear bands occur in the crushed sand fragment clusters, this leads to relative motions in the sand-steel interfaces which explains why coefficient of friction in the sand-steel contacts mainly determines the overall coefficient of adhesion.
- spheres with free rotation show no adhesion increasing effect, coefficient of friction in sand-sand and sand-steel contacts show only very little effect. In the case of hard surfaces, the adhesion coefficient can even be below the prescribed coefficient of friction for wet steel-steel contacts. It was supposed that this effect may results from some kind of roller bearing effect, but this hypothesis was falsified.
- analysing the shear force distributions in the sand-steel contacts acting in shear direction showed that in the case of rotating spheres a lot of contacts show forces in opposite direction to the resulting overall shear force which is not the case when the rotation of the speres is blocked. Although this results in even high mobilized friction coefficients, it reduces the overall adhesion coefficient.
- to obtain information about the ‘real’ behaviour of crushed sand fragments to be used for model development and calibration, a new testing methodology has been developed, a so called ‘mini shear box’ test rig.
- first tests have been carried out with different normal loads, and a coefficient of friction in the range of 0.3 – 0.55 was measured.
- the test rig is currently being improved, and further experiments are planned in future work so that the data then can be used for further model development, calibration and validation.

Acknowledgments

This research was funded in whole, or in part, by the Austrian Science Fund (FWF) project P 34273: DEM modelling of adhesion in sanded wheel-rail contacts. For the purpose of open access, the author has applied a CC BY public copyright licence to any Author Accepted Manuscript version arising from this submission. The publication was written at Virtual Vehicle Research GmbH in Graz and partially funded within the COMET K2 Competence Centers for Excellent Technologies by the Austrian Federal Ministry for Innovation, Mobility and Infrastructure (BMIMI), Austrian Federal Ministry for Economy, Energy and Tourism (BMWET), the Province of Styria (Dept. 12) and the Styrian Business Promotion Agency (SFG). The Austrian Research

Promotion Agency (FFG) has been authorised for the programme management.

Data Availability

The data set newly generated during the current study is openly available in the zenodo.org repository, see [18].

References

- [1] B. White, R. Lewis, *Simulation and understanding the wet-rail phenomenon using twin disc testing*, Tribology International, 136, 475–486, 2019.
- [2] G. Trummer, L. Buckley-Johnstone, P. Voltr, A. Meierhofer, R. Lewis, K. Six, *Wheel-rail creep force model for predicting water induced low adhesion phenomena*, Tribology International, 109, 409–415, 2017.
- [3] L. Buckley-Johnstone, G. Trummer, P. Voltr, A. Meierhofer, K. Six, D. Fletcher, R. Lewis, *Assessing the impact of small amounts of water and iron oxides on adhesion in the wheel/rail interface using High Pressure Torsion testing*, Tribology International, 135, 55–64, 2019.
- [4] W. Skipper, A. Chalisey, R. Lewis, *A review of railway sanding system research: adhesion restoration and leaf layer removal*, Tribology - Materials, Surfaces & Interfaces, 12, 237–251, 2018.
- [5] W. Skipper, A. Chalisey, R. Lewis, *A Review of Railway Sanding System Research: Wheel/Rail Isolation, Damage, and Particle Application*, Proceedings of the Institution of Mechanical Engineers. Part F: Journal of Rail and Rapid Transit, 2019.
- [6] S. Descartes, M. Renouf, N. Fillot, B. Gautier, A. Descamps, Y. Berthier, P. Demanche, *A new mechanical-electrical approach to the wheel-rail contact*, Wear, 265, 1408 – 1416, 2008.
- [7] C. Zhang, S. Maramizonouz, D. Milledge, S. Nadimi, *An electro-mechanical contact model for particulate systems*, Powder Technology, 440, 119759, 2024.
- [8] A. Gautam, S.I. Green, *Computational fluid dynamics–discrete element method simulation of locomotive sanders*, Journal of Rail and Rapid Transit, 235, 12–21, 2021.
- [9] S. Maramizonouz, S. Nadimi, W. Skipper, S. Lewis, R. Lewis, *Numerical modelling of particle entrainment in the wheel–rail interface*, Computational Particle Mechanics, 2023.
- [10] S. Maramizonouz, S. Nadimi, R. Lewis, *CFD-DEM modelling of particle entrainment in wheel–rail interface: a parametric study on train characteristics*, Acta Mech, 235, 6077–6087, 2024.
- [11] B. Zhang, S. Nadimi, R. Lewis, *Modelling the adhesion enhancement induced by sand particle breakage at the wheel-rail interface*, Wear, 538-539, 205232, 2024.
- [12] C. Zhang, S. Nadimi, S. Maramizonouz, D. Milledge, R. Lewis, *A Discrete Element Model of High-Pressure Torsion Test to Assess the Effect of Particle Characteristics in the Interface*, Journal of Tribology, 146, 081501, 2024.
- [13] P.A. Cundall, O.D.L. Strack, *A discrete numerical model for granular assemblies*, Geotechnique, 29(1), 47-65, 1979.
- [14] B. Suhr, W. A. Skipper, R. Lewis, K. Six, *Sanded Wheel-Rail Contacts: Experiments on Sand Crushing Behaviour*, Lubricants, 11, 2023.
- [15] B. Suhr, W. A. Skipper, R. Lewis, K. Six, *DEM simulation of single sand grain crushing in sanded wheel-rail contacts*, Powder Technology, 432, 2024.
- [16] B. Suhr, W. A. Skipper, R. Lewis, K. Six, *DEM modelling of surface indentations caused by granular materials: application to wheel–rail sanding*, Computational Particle Mechanics, 11, 2024.
- [17] B. Suhr, W. A. Skipper, R. Lewis, K. Six, *Mechanisms of adhesion increase in wet sanded wheel-rail contacts – a DEM based analysis*, Lubricants, under review, 2025.
- [18] B. Suhr, K. Six, W. Skipper, R. Lewis, *Mini shear box tests on crushed sand fragments under high normal stresses* [Data set], Zenodo, <https://doi.org/10.5281/zenodo.15479070>